

1 Carbon Accumulation in Mediterranean Rhodolith Beds during the 2 Holocene

3 Silvia de Juan¹, Ryan Smazal², Claudio Lo Iacono³, Maria del Mar Gil¹, Andrea Cabrito³, Andres Ospina-
4 Alvarez¹, Jorge Guillén³, Grace M. Cott², Laia Illa-López¹, Hilmar Hinz¹, Francesc Maynou³

5 ¹Instituto Mediterráneo de Estudios Avanzados IMEDEA (UIB-CSIC), c. Miquel Marquès 21, 07190
6 – Esporles (Spain)

7 ²School of Biology and Environmental Science, University College Dublin, Dublin, Ireland

8 ³Institut de Ciències del Mar (CSIC), Psg. Marítim de la Barceloneta 37-49, 08003-Barcelona (Spain)

9 *Correspondence to:* Silvia de Juan: silvia.dejuan@csic.es

10
11 **Abstract.** Rhodolith and maërl beds are globally relevant biogenic ecosystems whose long-term carbon
12 storage capacity remains poorly quantified, particularly in the Mediterranean. To fill this gap, we
13 investigated the formation, structure, and carbon content of a sediment deposit underlying a rhodolith
14 bed in the Menorca Channel (Western Mediterranean). High-resolution seismo-acoustic profiling
15 revealed a highly heterogeneous biogenic sedimentary deposit at ~60 m depth, with thickness ranging
16 from a few centimeters to 3.7 m (mean = 0.95 m). Seven cores extracted from the thickest sediment
17 deposits were analyzed for grain size, carbonate content, bioclast composition, organic carbon, and
18 radiocarbon age. Radiocarbon dating indicates that sediment accumulation began during the early
19 Holocene (11,700–9,000 yr BP), when post-glacial sea-level rise transitioned the area from subaerial
20 exposure to shallow-marine conditions. Despite the spatial limitation of collected data, several
21 conclusions could be drawn. Early deposits produced during the last sea-level rise were dominated by
22 bivalves and dispersed coralline fragments. The following establishment of modern sea level around
23 7,000–6,500 yr BP marks a change to the development of more stable dense rhodolith–maërl facies that
24 persist today. Sediment accretion rates are low (median = 8.54 cm kyr⁻¹), reflecting very low external
25 sediment supply, and slow growth of coralline algae. Organic carbon content in the upper 50 cm,
26 representing the most dynamic and recently deposited carbon pool, averaged 0.57% (± 0.22), with an
27 estimated organic carbon stock of 32.04 (± 4.18) Mg C ha⁻¹. These results show that rhodolith beds can
28 act as long-term organic carbon stores, forming spatially complex Holocene deposits that have been
29 largely overlooked.

30 **Keywords**

31 Calcareous red algae; sediment organic carbon; organic carbon sequestration; Holocene deposits;
32 paleoecology; Mediterranean Sea.

33 **Highlights**

- 34 • Seismo-acoustic mapping of a deep rhodolith deposit revealed highly variable thickness.
- 35 • Holocene sedimentation began 11,700–9,000 yr BP during post-glacial sea-level rise.
- 36 • Dense rhodolith–maërl facies formed after sea-level stabilization ~7,000 yr BP.
- 37 • Accretion rates are low (8.54 cm kyr⁻¹), very low external sediment supply and slow algal growth.
- 38 • Organic carbon averages 32.04 (± 4.18) Mg C ha⁻¹ in the upper 50 cm, of sediment.

39 1. INTRODUCTION

40 Marine ecosystems play an important role in the global carbon cycle by contributing to organic and
41 inorganic carbon storage. Coastal systems sequester atmospheric carbon dioxide (CO₂) through
42 photosynthesis and the subsequent burial of sedimentary organic carbon (Nellemann and Corcoran, 2009;
43 Barbier et al., 2011). Current evidence suggests that net organic carbon burial in the marine environment
44 comes from vegetated ecosystems such as mangroves, seagrass meadows and saltmarshes (Macreadie et
45 al., 2019). In contrast, calcifying algal systems such as rhodolith and maërl beds have received
46 considerably less attention, despite their global distribution and the millennial persistence of their
47 deposits. These characteristics suggests that they may represent an important, yet poorly quantified, long-
48 term carbon store (Aguirre et al., 2017; Tuya et al., 2023; Van der Heijden and Kamenos, 2015).

49 Rhodolith and maërl beds consist of free-living, non-geniculate calcareous red algae (Rhodophyta:
50 Corallinophycidae) that form multi-specific assemblages in subtidal environments. These habitats
51 typically occur on coarse mobile sediments under moderate hydrodynamic conditions that prevent burial
52 while maintaining sufficient irradiance (Aguirre et al., 2017; Basso et al., 2017; Bosence, 1983). Despite
53 their slow individual annual growth rates (~1 mm yr⁻¹), rhodolith accumulations can reach several meters
54 in thickness over hundreds to thousands of years. Living rhodoliths are restricted to the upper few
55 centimeters of the bed, overlying deposits of fragmented coralline algae and skeletal remains of
56 bryozoans, molluscs, and echinoderms (Fornós and Ahr, 1997; Betzler et al., 2011; Mao et al., 2020).

57 These long-lived carbonate-rich deposits may store carbon through both the accumulation of biogenic
58 sediments and the trapping of organic carbon supplied from external sources (Mao et al., 2020; Schubert
59 et al., 2024). The high particle-trapping capacity of rhodolith beds, driven by the three-dimensional
60 structural complexity of the algae, is a key mechanism underpinning this process (Mao et al., 2020; James
61 et al., 2024; Bulleri et al., 2025). This structure enhances the retention of suspended material, promoting
62 the accumulation of organic material and supporting carbon cycling within detritus-based food-webs
63 (Rendina et al., 2026). However, the broader role of rhodolith beds in carbon cycling remains uncertain,
64 as carbon storage through particle retention simultaneously occurs with calcium carbonate production, a
65 process that releases CO₂ (James et al., 2024a; Mao et al., 2024). Thus, in carbonate-dominated systems,
66 the balance between carbon burial and release of CO₂ is complex and not yet fully resolved (Macreadie
67 et al., 2019). For the purposes of this study, we focus specifically on quantifying sedimentary organic
68 carbon stocks and highlighting the potential for long-term storage, rather than resolving net ecosystem
69 carbon balance.

70 Large rhodolith and maërl beds are present on modern and ancient carbonate shelves across tropical to
71 polar regions (Riosmena-Rodríguez et al., 2017; Tuya et al., 2023), including the world's largest bed on
72 the Brazilian continental shelf (21 000 km², Amado-Filho et al., 2012). The Mediterranean hosts the
73 second-largest bed described to date, covering approximately 470 km² in the Menorca Channel, western
74 Mediterranean (Tabone et al., 2024). Its development has been facilitated by the clear waters and low
75 sediment input that characterize Mediterranean islands, allowing rhodolith beds to extend down to 90 m
76 depth (Joher et al., 2016). Despite their ecological importance, the capacity of Mediterranean rhodolith
77 beds to store sedimentary organic carbon over centennial to millennial timescales remains poorly
78 quantified. This is particularly true for the vertical distribution and spatial variability of carbon stocks,
79 as well as their relationship with deposit accretion history.

80 This knowledge gap is especially relevant given the high vulnerability of rhodolith beds to disturbance
81 due to their slow growth and limited recovery capacity. These habitats are threatened by bottom-contact
82 fishing gears, elevated suspended sediments, and the cumulative effects of ocean warming and
83 acidification under climate change (Tuya et al., 2023; Trégarot et al., 2024). Although Mediterranean
84 rhodolith beds are protected under EU Regulation 1997/2006, the EU Habitats Directive, and the
85 UNEP/MAP Action Plan (2008), effective management remains limited due to insufficient spatial
86 coverage and ecological data. Improving knowledge of their organic carbon storage capacity is essential
87 not only to clarify their contribution to the global carbon cycle, but also to strengthen the scientific basis
88 for conservation (de Macêdo Carneiro et al., 2021; Schubert et al., 2024).

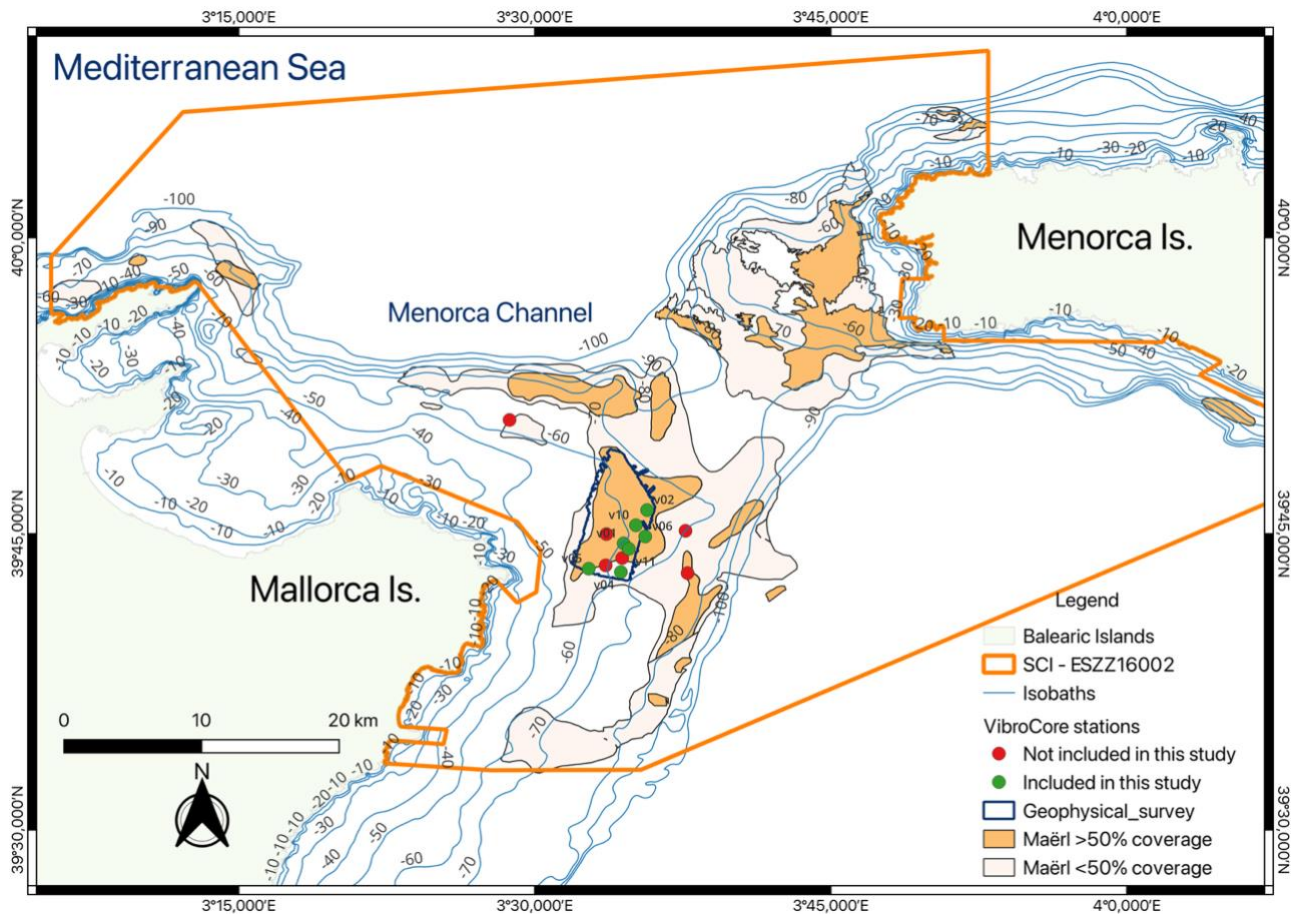
89 This study quantifies the role of Mediterranean rhodolith beds in long-term organic carbon storage by
90 analyzing sedimentary organic carbon deposition of a well-preserved deposit in the Menorca Channel
91 (western Mediterranean). The Menorca Channel is a temperate carbonate shelf where rhodolith sediments
92 have accumulated since the early Holocene, providing a unique archive to examine carbon storage over
93 millennial timescales. Using high-resolution seismo-acoustic data, sediment cores and radiocarbon
94 dating, we estimate the stock of organic carbon in the upper 50 cm of sediments. We test the hypothesis
95 that this rhodolith bed represents a consistent Holocene carbon store, shaped by local environmental
96 conditions and long-term sea-level changes, with implications for regional protection schemes for these
97 habitats.

98 2. MATERIAL AND METHODS

99 2.1. Study area

100 The Balearic continental shelf is a temperate, low-energy oligotrophic system dominated by carbonate-
101 producing habitats, including *Posidonia oceanica* meadows, coralligenous communities, and extensive
102 rhodolith–maërl beds (Canals and Ballesteros, 1997; Betzler et al., 2011). Our study focuses on the
103 Menorca Channel, a shallow carbonate platform (~100 m max depth) between Mallorca and Menorca,
104 where post-glacial neritic carbonates have accumulated since the early Holocene (Alonso et al., 1988;
105 Betzler et al., 2011). Rhodolith and maërl beds occur between 45–80 m depth on the platform (Fig. 1),
106 interspersed with detrital sands (de Juan et al., 2023). The preservation of these environments has been
107 assisted by a historical trawling exclusion zone surrounding nearby submarine cables and, more recently,
108 by the 2016 designation of the Menorca Channel as a Natura 2000 Site of Community Importance (SCI
109 ESZZ16002).

110 We focused on a 43.6 km² area where rhodolith and maërl cover exceeds 50%, based on high-resolution
111 mapping from the INDEMARES project (Moranta et al., 2014) and our own video surveys (Cabrito et
112 al., 2024b). Within this area, we conducted high-resolution seismo-acoustic profiling to determine the
113 thickness of bioclastic sediments above the acoustic basement and to identify suitable sites for recovering
114 ≥1-m sediment corers. Potential sites were inspected with a remotely operated vehicle (ROV) to confirm
115 rhodolith–maërl dominance, and full coverage was verified at all core locations.



116

117

118

119

120

121

122

123

Figure 1. Study area in the Menorca Channel, located between Mallorca and Menorca islands in the western Mediterranean Sea. The map shows the area covered by the geophysical survey (dark blue polygon) and the location of VibroCore stations included (green dots) and not included (red dots) in this study. Rhodoliths are represented in light and dark orange, indicating areas with 10-50% and >50% coverage, respectively. The Site of Community Importance (SCI ESZZ16002) is delineated by the dark orange boundary. Isobaths (in metres) are shown as blue contour lines. Source: modified from project INDEMARES (Moranta et al., 2014).

124

2.2. Geophysical map

125

126

127

128

129

130

131

132

In May 2022, we acquired 56 high-resolution seismo-acoustic profiles in the study area (Fig. 1) during a research cruise aboard R/V *SOCIB* and using an INNOMAR Medium-100 non-linear parametric echosounder coupled with an INS SBG Navisight Ekinox and GNSS AtlasLink for positioning. Sound-speed and turbidity corrections were obtained with a Valeport SWIFT. The system emits two primary frequencies around 100 kHz, producing a secondary frequency of 5–12 kHz, with a pulse repetition rate of up to 30 s⁻¹ and a beam width of ±1.8°. Non-linear parametric echosounders provide narrow, low-frequency beams with small footprints, enabling high-resolution imaging of shallow sediment deposits and precise localization of core-sampling (Lo Iacono et al., 2008).

133

134

Profiles were spaced 200 m apart, oriented NNE–SSW in the southern sector and NW–SE in the northern sector, intersected by perpendicular transversal profiles every 500–2000 m (Fig. A2, 3). Penetration depth

135 averaged 0.8–1.0 m and reached a maximum of 3.7 m, maintaining high horizontal and vertical metric
 136 to sub-metric resolution due to the small pulse size. Uncertainties were estimated to be of the order of \pm
 137 0.2 m. Seismo-acoustic data were interpreted using INNOMAR-ISE 2.9 to pick stratigraphic horizons
 138 and estimate thickness of the bioclastic deposit. Geo-referencing and isopach mapping were conducted
 139 with Global Mapper and ArcGIS.

140 2.3. Sediment core sampling

141 In May 2023, sediment cores were collected at 60–80 m depth during a research cruise aboard
 142 R/V *Sarmiento de Gamboa*. The coring sites were selected based on geo-acoustic evidence of maximum
 143 sediment thickness within the survey polygon (Fig. 2). A vibrocorer (ASTHER I, GEOMYTSA S.A.)
 144 operating at 136 kN centrifugal force at 3 m recovered 12 PVC-lined cores (9 cm diameter, 1.4–2.8 m
 145 length; Table 1). Each core was sectioned into ≤ 1 m segments and stored at -20 °C for laboratory
 146 analyses. Of the 12 cores, 7 were retained for this study; the remaining five cores were stored frozen for
 147 future genetic analysis to identify the presence of different species of rhodoliths (Fig. 1).

148 **Table 1** – Characteristics of the seven vibrocores obtained in the Menorca Channel (Western Mediterranean) selected for
 149 this study. Description of biocenoses based on knowledge from our own video observations and previous projects (Moranta
 150 et al., 2014).

| Vibrocore ID | Longitude | Latitude | Sea bottom Depth (m) | core length (m) | analyses | biocenose |
|--------------|-----------|----------|----------------------|-----------------|----------|---|
| V1 | 3.5750 | 39.7419 | 61.91 | 1.60 | + * # | rhodoliths >75%, with Peyssonnelia and Osmundaria |
| V2 | 3.5949 | 39.7700 | 66.22 | 1.40 | + * \$ # | rhodoliths >75%, with Laminaria |
| V4 | 3.5727 | 39.7177 | 66.08 | 1.80 | + * \$ # | rhodoliths >60%, with Osmundaria |
| V5 | 3.5456 | 39.7205 | 60.01 | 2.80 | + * # | rhodoliths >60%, with Osmundaria |
| V6 | 3.5933 | 39.7477 | 64.52 | 1.90 | + * \$ # | rhodoliths >60%, with Laminaria |
| V10 | 3.5854 | 39.7572 | 63.28 | 1.45 | + * # | rhodoliths >90%, with Peyssonnelia |
| V11 | 3.5794 | 39.7525 | 63.93 | 1.75 | + * \$ # | rhodoliths >75%, with Peyssonnelia |

151 + Lithology and clasts composition; * Granulometry and carbonates; \$ Radiocarbon dating; # Organic carbon

152

153 Sediment core opening and visual description

154 Each 1 m core section was cut longitudinally for analysis. All cores were visually inspected to describe
 155 sediment composition, and subsamples were collected for grain size, radiocarbon dating, bioclast
 156 identification, and organic carbon content analyses.

157 Grain size and carbonate contents

158 The cores were sampled at 5 cm intervals for grain-size and carbonate-content analyses. Grain-size
159 distributions were measured using a HORIBA LA-950V2 laser diffraction analyser after disaggregating
160 and removing the biogenic fraction (10% H₂O₂), and ultrasonic dispersion; the >2 mm fraction was
161 quantified by sieving. We calculated the weight percentages of clay, silt, sand, and gravel, as well as
162 mean grain size (ϕ), sorting (σ), skewness (Sk), and kurtosis (kG). Carbonate content was determined
163 from the CO₂ volume displaced by a sample of sediment treated with 20% HCl, calibrated against a 100%
164 CaCO₃ standard.

165 **Radiocarbon dating**

166 Between two and three bioclasts (rhodoliths or bivalve shells) from different depths in four cores (Table
167 1) were radiocarbon-dated by Beta Analytic (Miami, USA). Dates were calibrated with BetaCal 5.0, with
168 HPD method “MARINE20” and corrected for the local marine reservoir effect ($\Delta R = -112 \pm 99$).
169 Sediment accretion rates (cm kyr⁻¹) were calculated by dividing the thickness of sediment between
170 successive dated horizons along the core (kyr), taking the top most horizon as 0 yr BP.

171 **Taxonomic identification of bioclasts**

172 Sediment was examined under a binocular microscope at ~50 cm intervals for fauna identification.
173 Subsamples (10–20 g) were air-dried (48 h) and sieved through 0.5 and 1 mm meshes. Between 200 and
174 300 clasts from the >0.5–1 mm and >1 mm fractions were inspected and assigned to major taxonomic
175 groups (Bivalves, Gastropods, Bryozoans, Echinoids, Foraminiferans, and free-living coralline algae).
176 Rhodoliths were classified into two morphotypes following (Basso, 1998; Basso et al., 2012): non-
177 branched rhodoliths (including “boxwork” and “praline” forms; 1–5 cm) and branched maërl fragments
178 (0.5–2 cm) (see also Jardim et al., 2025; Teichert, 2024).

179 **2.4. Organic Carbon Content**

180 From each core, sediment samples (~21 ml) were collected using a syringe every 10 cm within the upper
181 50 cm, as this layer is expected to contain the highest and more dynamic carbon pool, which has not yet
182 undergone long-term diagenesis (Middelburg, 2018). To minimize decomposition of organic matter and
183 microbial growth, samples were kept cold (4 °C) during 24-48 hours for later processing. In the
184 laboratory, samples were weighed, freeze-dried (lyophilized) for 48-72 hours, and weighed again to
185 determine their moisture content percentage. Finally, the samples were finely ground in an agate ball
186 mill.

187 The processed samples were sent to University College Dublin to be sub-sampled for further analysis.
188 From each 10 cm layer, ~2.0 g (± 0.6 g) of homogenized sediment was subsampled for organic carbon
189 (OC) analysis. A sub-set of the homogenized sample was then shipped to the University of Waterloo
190 (Canada) for carbon and nitrogen analysis. The samples were analysed using an ECS 4010 Elemental
191 Analyzer (NC Technologies, Italy) coupled to a Delta Plus XL (Thermo-Finnegan, Germany) continuous
192 flow isotopic mass spectrometer (CRFIRMS). Samples were acid washed according to the University of
193 Waterloo Environmental Isotope Laboratory procedures in order to remove inorganic carbon and obtain
194 OC measurements. This included acid washing the sediments in HCl (10 ml of 10%) for 24 hours and
195 until the reaction subsided. The final OC value was determined using the measured OC percentage of the
196 acidified sample, which was normalized to the bulk sediment mass by multiplying by the samples non-
197 carbonate fraction. High effervescence during acid treatment indicated a substantial carbonate fraction,
198 resulting in a marked mass loss. The %C and %N was measured in bulk, analyzed against known certified
199 elemental standard materials. For QA/QC, sample replicates were analyzed every 8 to 10 samples, with
200 certified standard/reference materials comprising of at least 20% of every run. Analytical control
201 measures were based on the detection of major carbon (C) and nitrogen (N) peaks to ensure data
202 consistency and calibration accuracy.

203 **2.5. Data analysis**

204 To evaluate whether sediment characteristics control the density of retained OC, variation in OC density
205 (g/cm^3) was analysed in relation to sediment characteristics using linear mixed-effects models to account
206 for the hierarchical structure of the sampling design, with multiple depth subsamples collected within
207 each sediment core. Because OC density values were positive and right-skewed, the response was log-
208 transformed ($\log[\text{CarDens}]$) and modelled assuming Gaussian errors. Core identity was included as a
209 random intercept to accommodate non-independence among subsamples from the same core.

210 The following sediment characteristics, that were explored as candidate fixed effects, were: standardized
211 sediment depth (cm), median grain size (d_{50} ; μm), carbonate content (%), biogenic gravel content (%),
212 and sediment type (categorical). Owing to strong collinearity between d_{50} and the sand/silt fractions ($|r|$
213 ≈ 0.90 – 0.96), grain-size fractions were not included in models containing d_{50} . Potential residual
214 dependence within each corer along the depth profile was assessed by fitting models with a first-order
215 autoregressive correlation structure, AR(1). In addition, a random-slope formulation allowing core-
216 specific depth trends was tested using a diagonal random-effects structure (random intercept and depth
217 slope by core, with intercept–slope covariance constrained to zero). Models were compared using Akaike
218 Information Criteria, with maximum likelihood estimation used for model selection and the best-

219 supported model refitted by restricted maximum likelihood for final parameter estimation. The intraclass
220 correlation coefficient (ICC) was calculated from variance components to quantify the proportion of
221 variance attributable to differences among cores. All analyses were conducted in R v4.4.2.

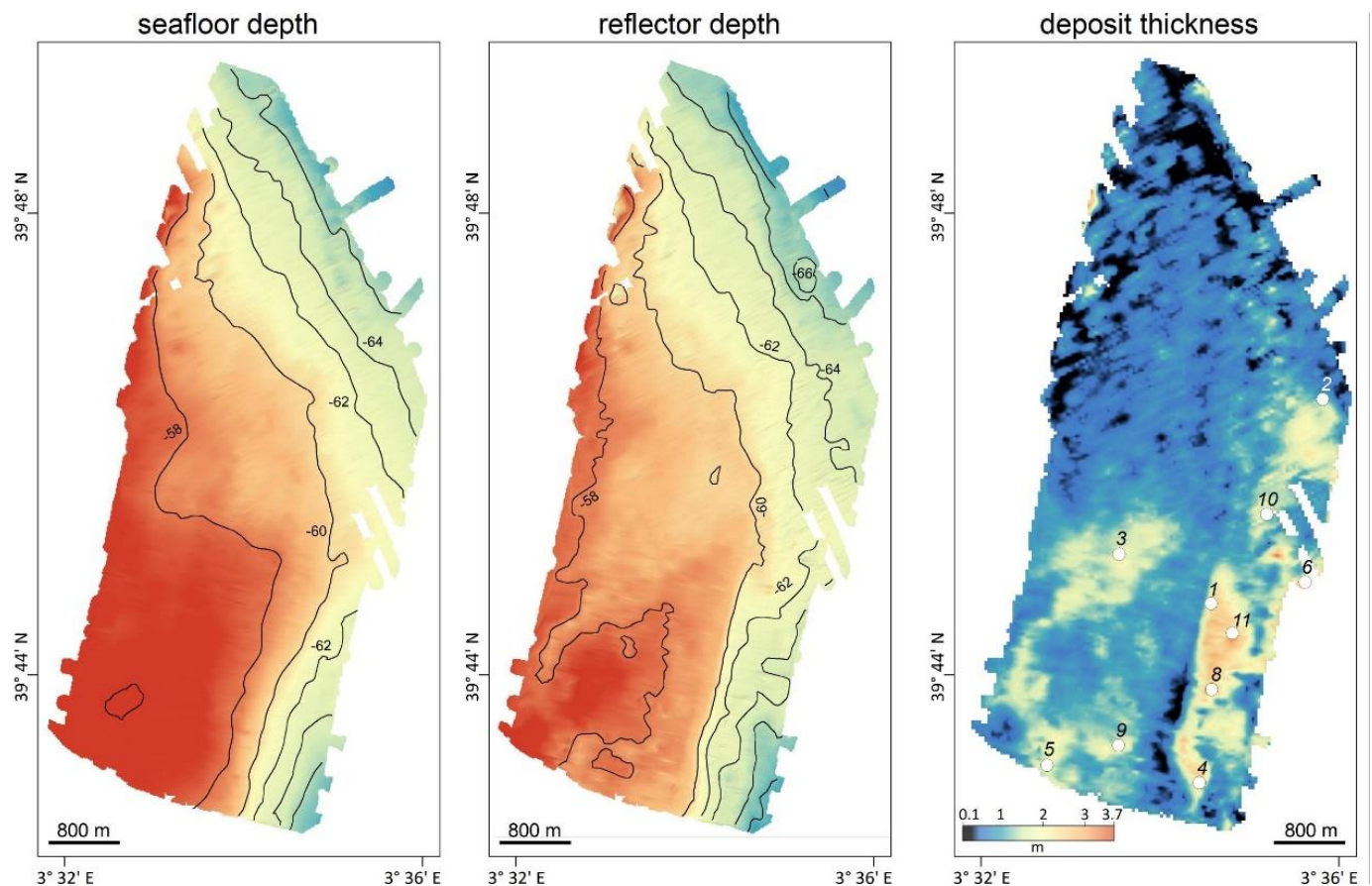
222 **3. RESULTS**

223 **3.1. Seismoacoustic records**

224 The surveyed area ranges from 57 to 68 m depth and exhibits generally smooth bathymetry, with an
225 average slope of 0.2°. The western sector is relatively flat, gradually deepening from 57 to 60 m, while
226 the southeast and northeast sections show narrow bathymetric edges with steeper slopes reaching 68 m
227 (Fig. 2).

228 Geo-acoustic profiles allowed detailed mapping of the 3D architecture of the bioclastic deposit. Sediment
229 thickness was highly heterogeneous at small scales, ranging from nearly 0 to several meters over spatial
230 extents of hundreds of meters or less (Fig. 2, right panel; Fig. A1). Average thickness was 0.95 m, with a
231 maximum of 3.7 m. Thinner deposits occurred in the northern sector (down to 10 cm), whereas thicker
232 accumulations were found in the southern and eastern sectors, including a 2 km × 1 km patch reaching
233 3.7 m at its depocenter.

234 Cores were collected at locations of maximum sediment accumulation. Of the seven cores retained for
235 this study, V1, V2, and V10 reached the bedrock horizon; V4, V6, and V11 fell short by 0.5–1.1 m; and
236 V5 slightly penetrated the bedrock (~1 m) (Figs. 2 and 3; Fig. A1).



237
238
239
240
241

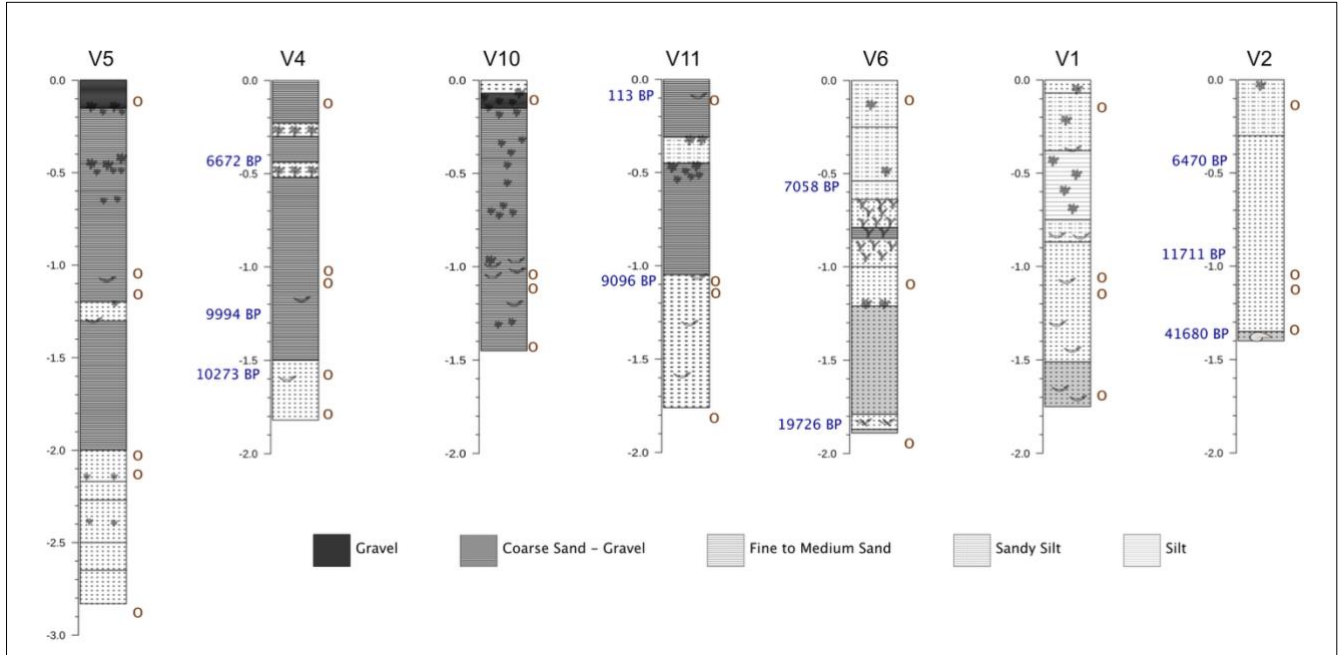
Figure 2. Results of the high-resolution profiling in the rhodolith deposit. Left panel: bathymetry, central panel: reflector depth, right panel: deposit thickness. Refer to position of geophysical survey in Fig. 1.

242 3.2. Sediment characteristics

243 Visual inspection of the cores revealed a relatively uniform composition, dominated by fine to coarse
244 bioclastic sand with occasional horizons of gravel or silt (Fig. 3; Fig. A4). Grain-size analysis confirmed
245 sand as the dominant fraction (>50%), with fines occasionally higher in certain horizons (e.g., V1: 40–
246 90 cm; V2: 30–60 cm; V4: 25–65 cm; V6: 25–60 cm; V11: 35–65cm), but never exceeding sand content.
247 Gravel was always <25%, with the exception of V5: 40–50 cm, 50% gravel. Carbonate contents were
248 consistently $\geq 90\%$ along the cores.

249 Sediment composition was primarily carbonate bioclasts (75%) and, to a lesser extent, carbonate
250 lithoclasts (8%), with variable contributions from siliciclastic grains. Stereomicroscope analysis allowed
251 identification of 65% of clasts, mainly unattached coralline red algae (26%, branched and non-branched),
252 bivalve fragments (22%), gastropods (13%), echinoid remains (4%), foraminifera (4%), and bryozoans
253 (3%). Minor groups included serpulids, ostracods, and polyplacophorans. Siliciclastic grains (17%) were
254 grey or white lithoclasts, distinguished by texture and lack of reaction to dilute HCl.

255 Coralline algae fragments occurred throughout the cores, whereas well-formed rhodoliths were confined
 256 to the upper ~60 cm (except V2), occurring either scattered or densely packed, particularly in V4, V5,
 257 and V11 (Fig. 3). Three cores (V1, V2, V6) terminated on cemented substrate, including bivalve-rich
 258 hardgrounds or reworked lithoclasts.



259 **Figure 3.** Stratigraphic columns showing the lithological composition of the sediment and radiocarbon dates (in blue).
 260 Circles: sampling for faunistic identification: ○ Clasts (only clasts > 5 cm are represented): non-branched rhodolith:
 261 branched rhodolith: entire bivalve shell: broken bivalve shell: rock fragment:

264 3.2.1. Radiocarbon Dating

265 Radiocarbon dating of rhodoliths and bivalve shells from four cores (Table 2) yielded ten age estimates.
 266 Two basal ages (41,680 yr BP in V2 and 19,726 yr BP in V6) indicate reworked pre-Holocene material
 267 from periods when the area was in an emerged sub-aerial setting. The next four oldest dates, between
 268 11,711 and 9,096 yr BP, correspond to the end of Younger Dryas (11,711 yr BP) and the subsequent rapid
 269 sea-level rise (until 9,000 yr BP), indicating that the area was a shallow marine environment (<20 m
 270 depth) dominated by bivalves and dispersed branched rhodoliths. Some lithoclasts within these horizons
 271 indicate continental input consistent with shallow-water conditions.

272 **Table 2.** Radiocarbon dates (¹⁴C) for carbonate bioclasts obtained from the testing laboratory of Beta Analytic (Miami, Fl.,
 273 US), recalibrated with BetaCal 5.0 and corrected for the local marine reservoir effect (-112 ± 99). * correspond to reworked
 274 ages
 275

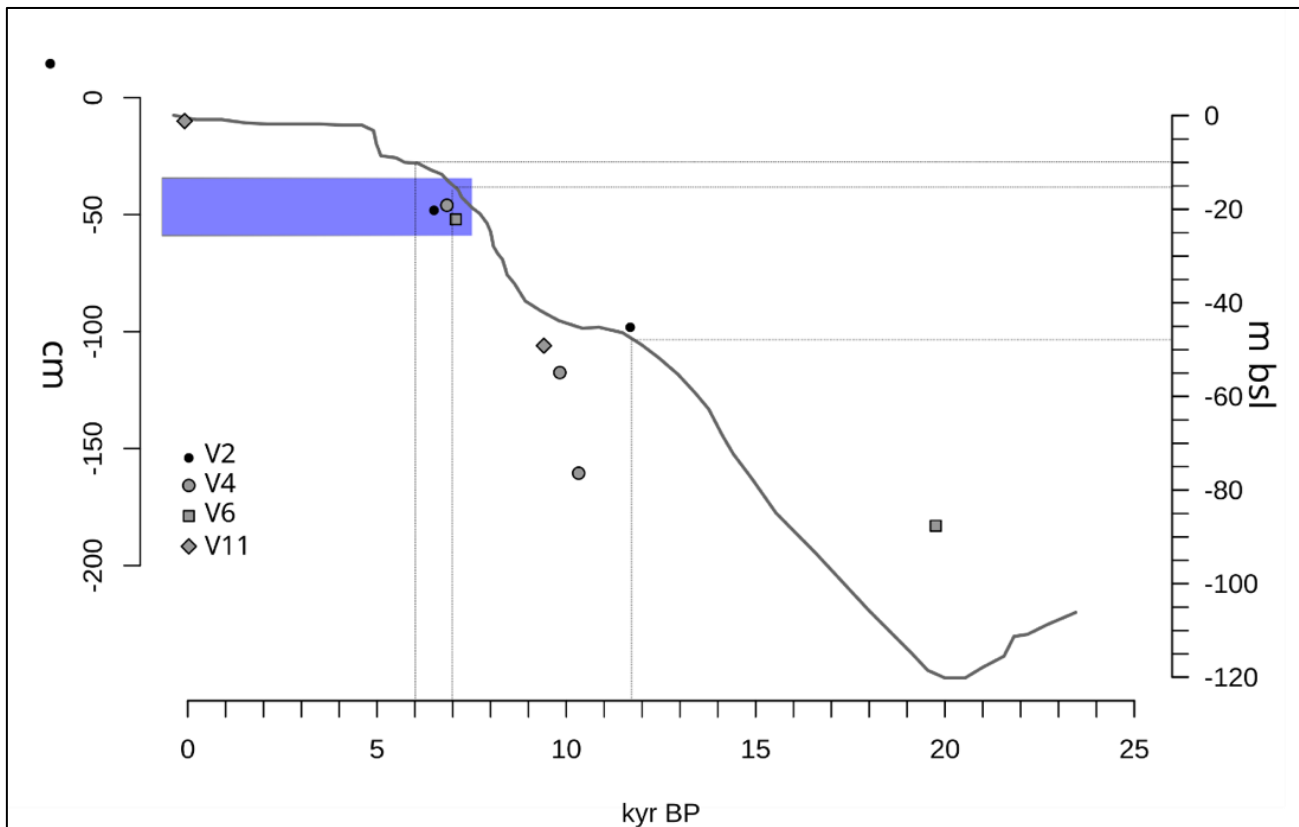
| Core | Depth (cm) | Radiocarbon Date BP | Calibrated Probability Data (2 sigma) | Calibrated years BP |
|------|------------|---------------------|---------------------------------------|---------------------|
| V2 | 136 | 37934 ± 875 | 41146-38315 BC 100% | 41680.5* |
| V2 | 97 | 10490 ± 30 | 10151-9371 BC 95.4% | 11711 |

| | | | | |
|-----|-------|-------------|--------------------|--------|
| V2 | 47 | 6110 ± 30 | 4778-4261 BC 95.4% | 6470 |
| V4 | 160.5 | 9460 ± 30 | 8640-8006 BC 95.4% | 10273 |
| V4 | 117.5 | 9270 ± 30 | 8372-7716 BC 95.4% | 9994 |
| V4 | 46 | 6300 ± 30 | 5000-4444 BC 95.4% | 6672 |
| V6 | 183 | 28067 ± 392 | 30634-4918 BC 100% | 19726* |
| V6 | 52 | 6552 ± 81 | 5298-4918 BC 100% | 7058 |
| V11 | 106 | 8530 ± 30 | 7455-6837 BC 95.4% | 9096 |
| V11 | 10 | 340 ± 30 | 1724-1950 BD 95.4% | 113 |

276

277 Three younger ages, between 7,058 and 6,470 yr BP (47–52 cm depth in V2, V4, and V6), correspond to
 278 a period when the Menorca Channel was ~10–15 m below present sea level, during which well-formed,
 279 densely packed rhodoliths accumulated (Fig. 3). During this interval, continental inputs diminished,
 280 maërl became abundant, and rhodolith beds consolidated, as exemplified by V4 (~50 cm, 6,672 yr BP).
 281 Scattered rhodolith fragments occasionally occur at greater depths, but none are found in strata older than
 282 9,096 yr BP, highlighting the onset of persistent rhodolith accumulation after postglacial transgression.

283 Based on these dates, sediment accretion rates range from 6.9 to 21.5 cm kyr⁻¹, with a median of 8.54
 284 cm kyr⁻¹ (Fig. 4).



285

286

287

288

Figure 4. Age-depth plot for the dated cores (excluding one sample that yielded a date > 40 ky BP) from the rhodolith deposit of the Menorca channel. Sea-level height (m) relative to present day based on the average model from (Bianchi et

289 al., 2012), largely based on results from (Lambeck and Bard, 2000). Relevant dates for this deposit (end of Younger Dryas at
 290 11700 yr BP and period of sea level stabilization between 7000 and 6000 yr BP) are marked along the x-axis and the
 291 corresponding depth below current sea level on the right y-axis. Blue stripe between 35 and 60 cm core depth shows the
 292 onset of horizons with high abundance of rhodoliths.
 293

294 3.3. Organic Carbon content

295 The average OC content in the upper 50 cm of sediment across all cores was 0.57% (± 0.22) (Table 3).
 296 OC content showed little variation with depth within this interval (Table A1). Using these measurements,
 297 OC stocks were determined for each core. Over the first 30 cm, we estimate an average across all the
 298 cores of 19.41 (± 4.42) Mg C ha⁻¹. Over the full 50 cm, we estimate an OC stock of 32 (± 4.18) Mg C
 299 ha⁻¹ across all the cores (Table 3).

300 In order to estimate annual OC accumulation, the 50 cm stock (3,200 g C m⁻²) was divided by the
 301 approximate age of the 50 cm horizon. Considering a median sediment accretion rate of 8.54 cm kyr⁻¹,
 302 annual OC accumulation is estimated at 0.546 g C m⁻² yr⁻¹. These estimates should be treated with
 303 caution, bearing in mind that the sediment cores were extracted from the points of greatest sediment
 304 accumulation (Fig. 2). Furthermore, this also assumes a constant sediment accumulation over time and
 305 does not account for potential hiatuses or erosional activity, thus representative of a long-term historical
 306 estimate rather than flux.

307 The molar C/N ratios were used to assess the origin and degree of degradation of the organic matter. The
 308 average C/N ratio across all samples was 10.71 (+/-3.19), with the highest value being 18.51 (V11) and
 309 the lowest value being 7.71 (V4) indicating predominantly marine sources.

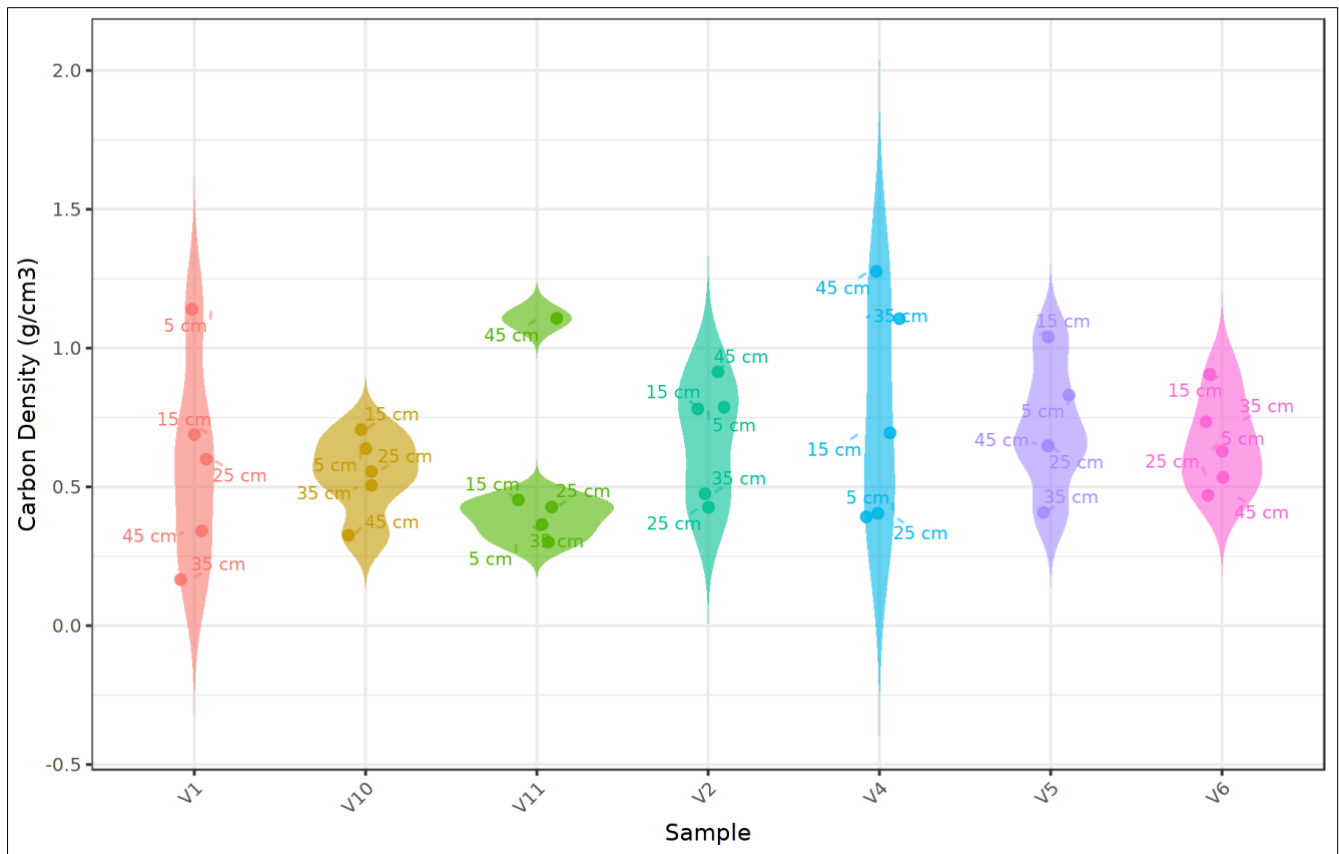
310 **Table 3.** Summary table showing the average organic carbon density, the stock over the top 30 and 50 cm of the cores.
 311

| Core | Avg C Density (kg C m ⁻³) | Carbon Stock Top 30 cm (Mg C ha ⁻¹) | Carbon Stock 50 cm (Mg C ha ⁻¹) |
|-----------|--|--|--|
| V1 | 5.87 | 24.28 | 29.36 |
| V2 | 6.77 | 19.94 | 31.3 |
| V4 | 7.75 | 14.92 | 38.74 |
| V5 | 7.15 | 25.19 | 31.4 |
| V6 | 6.54 | 20.68 | 31.7 |
| V10 | 5.46 | 18.99 | 27.31 |
| V11 | 5.031 | 11.82 | 31.6 |
| All Cores | 6.41 | 19.41 | 32.04 |
| | | | 31.7 |

318

319 Mixed-effects modelling indicated that OC density in the upper 50 cm was primarily explained by
320 carbonate content and grain size (d50), with a weaker contribution from biogenic gravel content, while
321 depth within the core showed no consistent effect. Alternative model structures, including sediment type,
322 random slopes for depth, and AR(1) correlation across depth, did not improve model fit and were not
323 retained (see Table A2, A3). In the final model, d50 was positively associated with OC density ($\beta = 0.177$,
324 $p = 0.0046$) and carbonate was negatively associated with OC density ($\beta = -0.306$, $p < 0.001$), whereas
325 biogenic gravel showed a weaker positive association ($\beta = 0.098$, $p = 0.0688$) and depth was not
326 significant ($p = 0.577$). Approximately 42% of the variability in OC density was attributable to
327 differences among cores, with the remaining variance occurring within cores and as unexplained residual
328 variability (Fig. 5).

329



330

331 **Figure 5.** Organic carbon density in the sediments (g/cm³) of the first 50 cm of cores.
332

332

333 4. DISCUSSION

334 The Holocene sedimentary deposit underlying the present-day rhodolith bed in the Menorca Channel
335 reflects a highly dynamic environment shaped by post-glacial sea-level rise. The deposit rests on an
336 erosional unconformity that likely incorporates reworked Miocene–Pliocene materials (Guillén, 1987).
337 The pronounced spatial variability observed among corers, even over relatively short distances, suggests
338 that local paleo-topography has exerted a strong control on sediment accumulation. Similar patterns have
339 been reported from other temperate carbonate shelves, where interactions between seabed morphology
340 and hydrodynamic conditions generate a complex mosaic of erosion, transport and deposition (Betzler et
341 al., 2011; Fornós and Ahr, 1997). These processes have likely shaped the present bioclastic landscape of
342 the Menorca Channel and contributed to the long-term persistence of rhodolith-rich habitats. Importantly,
343 the heterogeneous distribution of sediments indicates that organic carbon storage is unlikely to be
344 uniform across the bed. Consequently, reliable estimates of carbon stocks will require extending
345 geophysical surveys and sediment sampling to capture this spatial variability.

346 Radiocarbon data suggests that rhodolith assemblages in the Menorca Channel established during the
347 Early Holocene and developed under conditions comparable to other mid- to late-Holocene shallow
348 marine carbonate systems. Their timing placed them between younger maërl deposits in western France
349 (5,860–5,300 yr BP, Ehrhold et al., 2021) and older rhodolith beds reported from the Gulf of Mexico
350 (13,886 yr BP, Olmstead and Andrus, 2024), although such comparisons should be interpreted cautiously
351 given regional differences in environmental and depositional settings. Within the Menorca Channel
352 records, sediment deposits formed at the end of the Younger Dryas and during rapid postglacial sea-level
353 rise (~9000 yr BP onwards) are characterized by bivalves-dominated assemblages with dispersed
354 branched rhodoliths. The interpretation of the lower and older sections of the cores is complicated by
355 evidence of reworked deposits; nevertheless, the data suggests that well-formed rhodoliths most probably
356 established later (upper ~60 cm of sediment, around 7,000–6,000 yr BP), with more stable marine
357 conditions, coinciding with sea-level stabilization near present-day levels (Lambeck, 1995). This
358 transition marks the onset of dense rhodolith beds characterised by large, tightly packed rhodoliths, with
359 branched and boxwork morphologies, whose expansion and long-term persistence were likely favored
360 by moderate hydrodynamics, reduced terrigenous input, and mesophotic conditions that limit competitive
361 pressure (Aguirre et al., 2012; Basso et al., 2017). This continued presence over 6000 years highlights
362 the capacity of these systems to maintain structural complexity in the long-term, with potential

363 implications for their role as long-term organic carbon deposits, and for their conservation and
364 management.

365 Present-day seafloor patterns in the Menorca Channel are characterized by patches of rhodoliths
366 occurring at high densities (50–100% surface coverage), ranging in size from ~10 m² to over 100 m², and
367 predominantly composed of branched forms (Cabrito et al., 2024a, b). This spatial heterogeneity is
368 consistent with observations from other deep Mediterranean rhodolith beds (Rendina et al., 2020; Bracchi
369 et al., 2022; Tabone et al., 2024). Sediments are consistently carbonate-rich and dominated by bioclastic
370 material, with relatively uniform organic carbon content in the upper layers. In contrast, sediment
371 thickness is highly heterogeneous at small spatial scales. Reflecting these patterns, mixed-effects
372 modelling indicated that approximately 42% of the variability in organic carbon density was attributable
373 to differences among cores, suggesting small-scale patchiness in carbon accumulation across the
374 rhodolith bed that may be linked to local patchiness in rhodolith morphology and accumulation. Spatial
375 heterogeneity, together with variability in rhodolith density and morphology, may influence particle
376 trapping capacity and organic carbon retention (Cabrito et al., 2024a; Neto et al., 2021); however, this
377 remains to be evaluated, as the cores analysed were collected in the deepest sediment deposits from the
378 main rhodolith patch characterized by high cover and structural complexity. Organic carbon density was
379 largely controlled by sediment composition (grain size and carbonate content), consistent with dilution
380 in carbonate-rich sediments and a textural control on carbon storage (Howard et al., 2018; Keil et al.,
381 1994). The absence of a depth effect suggests relatively uniform near-surface conditions, consistent with
382 active bioturbation and hydrodynamic reworking that promote sediment mixing.

383 The relatively uniform organic carbon content in the upper 50 cm of sediment suggests low degradation
384 rates over the last ~6,000 years, coinciding with sea level stabilization. This stability likely favored the
385 development of well-formed rhodolith ecosystems, facilitating organic carbon capture and long-term
386 retention. Based on our estimates, these sediments store approximately 32.04 Mg C ha⁻¹ in the upper 50
387 cm, with an average of 19.41 (± 4.42) Mg C ha⁻¹ in the upper 30 cm. Using an estimated sediment
388 accretion rate of 8.54 cm kyr⁻¹, this corresponds to an average organic carbon accumulation of ~0.546 g
389 C m⁻² yr⁻¹. These values exceed previous estimates reported for coralline algal beds in temperate coastal
390 environments. For example, Mao et al. (2020) reported average organic carbon stocks of 7.23 ± 1.30 Mg
391 C ha⁻¹ within the upper 25 cm and 12.28 ± 1.98 Mg C ha⁻¹ across the full depth of carbonate deposits
392 (~80 cm) in Scottish coastal rhodolith beds. The substantially higher carbon stocks observed in the
393 Menorca deposit likely reflect differences in the environmental context: extending to mesophotic depths

394 it allows long-term depositional stability and slow sediment turnover. Rather than acting as a rapid carbon
395 sink, this system would serve as a millennial-scale carbon reservoir, preserving organic matter within a
396 very slowly forming carbonate matrix. Nevertheless, future work should investigate deeper sediment
397 layers (>50 cm), to determine the depth and age at which organic carbon mineralized. This would also
398 help to clarify the role of spatial heterogeneity in the deposit, and whether areas with thinner sediment
399 cover differ in their capacity for carbon retention.

400 The relatively high organic carbon stocks documented in the Menorca Channel reinforce growing
401 evidence that rhodolith beds can contribute to long-term carbon storage despite their slow sediment
402 accretion rates (Mao et al., 2024; Van Der Heijden and Kamenos, 2015). The persistence of organic
403 carbon observed in these deposits reflects two complementary processes: the long-term preservation of
404 organic matter within slowly accumulating sediments and the longevity of coralline algal systems, whose
405 carbonate skeletons resist degradation and maintain biogenic habitats over millennial timescales (Aguirre
406 et al., 2000; Van Der Heijden and Kamenos, 2015; Wilson et al., 2004). The three-dimensional structure
407 of rhodolith beds promotes the trapping and burial of suspended organic matter, including allochthonous
408 carbon, while low remineralization rates favour its preservation over long timescales (James et al.,
409 2024b). While rhodolith beds can store substantial amounts of organic carbon, their net contribution to
410 climate mitigation remains an open question because the balance between carbon burial and calcification-
411 related carbon release is not yet fully resolved (Kamenos et al., 2013; Mao et al., 2024; Schubert et al.,
412 2024; Van Der Heijden and Kamenos, 2015). Within this context, Blue Carbon frameworks have focused
413 on mangroves, salt marshes, and seagrass meadows. However, coralline algal beds are increasingly
414 recognized as non-classical Blue Carbon ecosystems because of their capacity to store organic carbon
415 over centennial to millennial timescales (James et al., 2024a). While their annual accumulation rates are
416 relatively low, their extensive global distribution and long-term persistence suggest that their cumulative
417 contribution to coastal carbon storage may be substantial (Van Der Heijden and Kamenos, 2015). The
418 carbon stocks quantified in the Menorca Channel support this emerging perspective and highlight the
419 importance of protecting these ecosystems, as disturbance can rapidly mobilize carbon deposits that have
420 accumulated over millennia.

421 The extremely low sediment accretion rates make these organic carbon deposits highly vulnerable to
422 physical disturbance, particularly from bottom-contact fishing such as trawling and dredging (Trégarot
423 et al., 2024). These activities can fragment nodules, bury living rhodoliths, and alter the structure and
424 compaction of the sediment, with impacts that persist over timescales far longer than ecosystem

425 management schemes (de Juan et al., 2013; Cabanellas-Reboredo et al., 2018; Tauran et al., 2020). The
426 upper few centimeters of the deposit can be disrupted by a single trawl passage, not only halting carbon
427 sequestration but potentially remobilizing organic carbon that accumulated over thousands of years
428 (Bernard et al., 2019). In the Mediterranean, many rhodolith beds remain exposed to such pressures, as
429 they alternate with soft-sediment ecosystems exposed to commercial trawling (de Juan et al., 2013; Illa-
430 López et al., 2023). In contrast, the Menorca Channel deposit has been protected from trawling due to
431 the historical presence of submarine communication cables. Evidence from this less disturbed site
432 suggests relatively uniform carbon preservation and burial under natural, undisturbed conditions. This
433 evidence highlights the need for future research into rhodolith beds. In particular, this would include
434 assessing whether organic carbon trapped by rhodolith beds, as opposed to carbon produced via rhodolith
435 calcification, is sequestered at rates that balanced or exceed calcification-related carbon release. This
436 highlights the critical role of protection in maintaining the long-term carbon storage and ecological
437 integrity of rhodolith ecosystems.

438 **Conclusions**

439 Rhodolith beds in the western Menorca Channel form the surficial sedimentary layer over a Holocene
440 depositional framework and constitute long-term sedimentary carbon archives within carbonate shelf
441 systems. Their organic carbon content remains relatively stable through the upper 50 cm, indicating
442 sustained accumulation and limited degradation over ~6,000 years. This persistence is enabled by the
443 three-dimensional structure of rhodoliths, which promotes sediment trapping and long-term carbon
444 preservation despite slow accretion rates, supporting their role as long-term carbon reservoirs rather than
445 rapid carbon sinks. These systems have persisted despite environmental changes, including human
446 impacts, yet their slow growth and sensitivity to physical disturbance make them highly vulnerable.
447 Protecting rhodolith beds from trawling and dredging is essential not only for biodiversity conservation
448 but also for maintaining their function as long-term carbon stores and reinforcing their contribution to
449 climate regulation. These findings suggest that carbonate biogenic systems such as rhodolith beds should
450 be reconsidered as long-term carbon repositories within blue carbon frameworks.

451 **Author contributions**

452 SdJ, FM, and CL conceptualized the study. AC, MdMG, SdJ, RS, and LI conducted sample collection
453 and processing. MdMG and CL curated the data. SdJ, RS, and AO performed the formal analysis. CL,

454 RS, and AO developed the methodology. SdJ, FM, and CL prepared the original draft of the manuscript.
455 HH, JG, and GC contributed to reviewing and editing the manuscript. SdJ, FM, and GC acquired funding.

456 **Competing interests**

457 The authors declare that they have no conflict of interest.

458 **Code and data availability**

459 The data supporting the findings of this study, including sediment core descriptions, geochemical
460 analyses, and radiocarbon dates, are available from the corresponding author upon reasonable request.

461 **Acknowledgements**

462 The authors would like to thank the crew of the R/V SOCIB and R/V Sarmiento de Gamboa during the
463 research cruises, partly funded by the Spanish Ministry of Science and Innovation. We thank the
464 companies NAUTILUS and GEOMYTSA for their technical support during field work to obtain
465 geophysical maps and vibrocores.

466 **Financial Support**

467 This work was funded by EU Horizon project MARBEFES (contract no. 101060937) and RHODOMED
468 (Spanish Ministry of Science grant nº PID2023-146998OB-C22). This work contributes to IMEDEA's
469 'Center of Excellence' Maria de Maetzu (CEX2021-001198) and ICM's 'Center of Excellence' Severo
470 Ochoa (CEX2019-000928-5). The Spanish Ministry of Science and Innovation supported S.d.J. with a
471 "Ramón y Cajal" grant (RyC2020-029062-I), A.O.-A. with a "Ramon y Cajal" grant (RyC2023-043454-
472 I) and L.I.-L with a FPI predoctoral (PRE2022-104567).

473 **References**

474 Aguirre, J., Riding, R., and Braga, J. C.: Diversity of coralline red algae: origination and extinction
475 patterns from the Early Cretaceous to the Pleistocene, *Paleobiology*, 26, 651–667, 2000.

476 Aguirre, J., Braga, J. C., MArtín, J. M., and Betzler, C.: Palaeoenvironmental and stratigraphic
477 significance of Pliocene rhodolith beds and coralline algal bioconstructions from the Carboneras Basin
478 (SE Spain), *Geodiversitas*, 34, 115–136, 2012.

479 Aguirre, J., Braga, J. C., and Bassi, D.: Rhodoliths and rhodolith beds in the rock record, in:
480 *Rhodolith/maërl beds: A global perspective*, Springer, 105–138, 2017.

481 Alonso, B., Guillén, J., Canals, M., Serra, J., Acosta, J., Herranz, P., Sanz, J. L., Calafat, A., and
482 CATAFAU, A.: Los sedimentos de la plataforma continental balear, *Acta Geológica Hispánica*, 185–
483 196, 1988.

- 484 Amado-Filho, G. M., Moura, R. L., Bastos, A. C., Salgado, L. T., Sumida, P. Y., Guth, A. Z., Francini-
485 Filho, R. B., Pereira-Filho, G. H., Abrantes, D. P., Brasileiro, P. S., Bahia, R. G., Leal, R. N., Kaufman,
486 L., Kleypas, J. a, Farina, M., and Thompson, F. L.: Rhodolith beds are major CaCO₃ bio-factories in
487 the tropical South West Atlantic., *PloS ONE*, 7, e35171, <https://doi.org/10.1371/journal.pone.0035171>,
488 2012.
- 489 Barbier, E. B., Hacker, S. D., Kennedy, C. J., Koch, E. W., Stier, A. C., and Silliman, B. R.: The value
490 of estuarine and coastal ecosystem services, *Ecological Monographs*, 81, 169–193, 2011.
- 491 Basso, D.: Deep rhodolith distribution in the Pontian Islands, Italy: a model for the paleoecology of a
492 temperate sea, *Palaeogeography, palaeoclimatology, palaeoecology*, 137, 173–187, 1998.
- 493 Basso, D., Caragnano, A., Benzoni, F., Rodondi, G., and others: Southern Sinai rhodoliths: facies,
494 species composition, and growth rate (Red Sea, Egypt), in: *International rhodolith workshop*, 2012.
- 495 Basso, D., Babbini, L., Ramos-Esplá, A. A., and Salomidi, M.: Mediterranean rhodolith beds,
496 *Rhodolith/Maërl Beds: a global perspective*, 281–298, 2017.
- 497 Bernard, G., Romero-Ramirez, A., Tauran, A., Pantalos, M., Deflandre, B., Grall, J., and Grémare, A.:
498 Declining maerl vitality and habitat complexity across a dredging gradient: insights from in situ
499 sediment profile imagery (SPI), *Scientific Reports*, 9, 16463, 2019.
- 500 Betzler, C., Braga, J. C., JARAMILLO-VOGEL, D., Roemer, M., Huebscher, C., Schmiedl, G., and
501 Lindhorst, S.: Late Pleistocene and Holocene cool-water carbonates of the Western Mediterranean Sea,
502 *Sedimentology*, 58, 643–669, 2011.
- 503 Bianchi, C. N., Morri, C., Chiantore, M., Montefalcone, M., Parravicini, V., Rovere, A., and others:
504 Mediterranean Sea biodiversity between the legacy from the past and a future of change, *Life in the*
505 *Mediterranean Sea: a look at habitat changes*, 1, 55, 2012.
- 506 Bosence, D. W.: The occurrence and ecology of recent rhodoliths—a review, *Coated grains*, 225–242,
507 1983.
- 508 Bracchi, V. A., Caronni, S., Meroni, A. N., Burguett, E. G., Atzori, F., Cadoni, N., Marchese, F., and
509 Basso, D.: Morphostructural characterization of the heterogeneous rhodolith bed at the marine
510 protected area “capo carbonara”(Italy) and hydrodynamics, *Diversity*, 14, 51, 2022.
- 511 Bulleri, F., Schubert, N., Hall-Spencer, J. M., Basso, D., Burdett, H. L., Francini-Filho, R. B., Grall, J.,
512 Horta, P. A., Kamenos, N. A., Martin, S., and others: Positive species interactions structure rhodolith
513 bed communities at a global scale, *Biological Reviews*, 100, 428–444, 2025.
- 514 Cabanellas-Reboredo, M., Mallol, S., Barberá, C., Vergés, A., Díaz, D., and Goñi, R.: Morpho-
515 demographic traits of two maërl-forming algae in beds with different depths and fishing histories.,
516 *Aquatic Conservation*, 28, 2018.
- 517 Cabrito, A., de Juan, S., Hinz, H., and Maynou, F.: Morphological insights into the three-dimensional
518 complexity of rhodolith beds, *Marine Biology*, 171, 127, 2024a.

- 519 Cabrito, A., Maynou, F., Simide, R., Mouillot, D., Lossent, J., and de Juan, S.: Non-extractive fish
520 diversity assessment in Mediterranean rhodolith beds, *Aquatic Conservation: Marine and Freshwater*
521 *Ecosystems*, 34, e4212, 2024b.
- 522 Canals, M. and Ballesteros, E.: Production of carbonate particles by phytobenthic communities on the
523 Mallorca-Menorca shelf, northwestern Mediterranean Sea, *Deep Sea Research Part II: Topical Studies*
524 *in Oceanography*, 44, 611–629, 1997.
- 525 Ehrhold, A., Jouet, G., Le Roy, P., Jorry, S. J., Grall, J., Reixach, T., Lambert, C., Gregoire, G., Goslin,
526 J., Roubi, A., and others: Fossil maerl beds as coastal indicators of late Holocene palaeo-environmental
527 evolution in the Bay of Brest (Western France), *Palaeogeography, Palaeoclimatology, Palaeoecology*,
528 577, 110525, 2021.
- 529 Fornós, J. J. and Ahr, W.: Temperate carbonates on a modern, low-energy, isolated ramp; the Balearic
530 platform, Spain, *Journal of Sedimentary Research*, 67, 364–373, 1997.
- 531 Guillén, J.: La sedimentación carbonatada en la plataforma continental de Campos (Sur de Mallorca),
532 1987.
- 533 Howard, J. L., Creed, J. C., Aguiar, M. V., and Fourqurean, J. W.: CO₂ released by carbonate sediment
534 production in some coastal areas may offset the benefits of seagrass “Blue Carbon” storage, *Limnology*
535 *and Oceanography*, 63, 160–172, 2018.
- 536 Illa-López, L., Cabrito, A., de Juan, S., Maynou, F., and Demestre, M.: Distribution of rhodolith beds
537 and their functional biodiversity characterisation using ROV images in the western Mediterranean Sea,
538 *Science of the Total Environment*, 905, 167270, 2023.
- 539 James, K., Macreadie, P. I., Burdett, H. L., Davies, I., and Kamenos, N. A.: It’s time to broaden what
540 we consider a ‘blue carbon ecosystem,’ *Global Change Biology*, 30, e17261, 2024a.
- 541 James, K., Macreadie, P. I., Burdett, H. L., Davies, I., and Kamenos, N. A.: It’s time to broaden what
542 we consider a ‘blue carbon ecosystem,’ *Global Change Biology*, 30, e17261, 2024b.
- 543 Jardim, V. L., Grall, J., Barros-Barreto, M. B., Bizien, A., Benoit, T., Braga, J. C., Brodie, J., Burel, T.,
544 Cabrito, A., Diaz-Pulido, G., and others: A common terminology to unify research and conservation of
545 coralline algae and the habitats they create, *Aquatic Conservation: Marine and Freshwater Ecosystems*,
546 35, e70121, 2025.
- 547 Joher, S., Ballesteros, E., and Rodríguez-Prieto, C.: Macroalgal-dominated coastal detritic communities
548 from the Western Mediterranean and the Northeastern Atlantic, *Mediterranean Marine Science*, 17,
549 476–495, 2016.
- 550 de Juan, S., Lo Iacono, C., and Demestre, M.: Benthic habitat characterisation of soft-bottom
551 continental shelves: Integration of acoustic surveys, benthic samples and trawling disturbance intensity,
552 *Estuarine, Coastal and Shelf Science*, 117, 199–209, <https://doi.org/10.1016/j.ecss.2012.11.012>, 2013.
- 553 de Juan, S., Ospina-Alvarez, A., Hinz, H., Moranta, J., and Barberá, C.: The continental shelf seascape:
554 a network of species and habitats, *Biodiversity and Conservation*, 1–20, 2023.

- 555 Kamenos, N. A., Burdett, H. L., Aloisio, E., Findlay, H. S., Martin, S., Longbone, C., Dunn, J.,
556 Widdicombe, S., and Calosi, P.: Coralline algal structure is more sensitive to rate, rather than the
557 magnitude, of ocean acidification, *Global Change Biology*, 19, 3621–3628, 2013.
- 558 Keil, R. G., Tsamakis, E., Fuh, C. B., Giddings, J. C., and Hedges, J. I.: Mineralogical and textural
559 controls on the organic composition of coastal marine sediments: Hydrodynamic separation using
560 SPLITT-fractionation, *Geochimica et Cosmochimica Acta*, 58, 879–893, 1994.
- 561 Lambeck, K.: Late Pleistocene and Holocene sea-level change in Greece and south-western Turkey: a
562 separation of eustatic, isostatic and tectonic contributions, *Geophysical Journal International*, 122,
563 1022–1044, 1995.
- 564 Lambeck, K. and Bard, E.: Sea-level change along the French Mediterranean coast for the past 30 000
565 years, *Earth and Planetary Science Letters*, 175, 203–222, 2000.
- 566 Lo Iacono, C., Mateo, M. A., Gracia, E., Guasch, L., Carbonell, R., Serrano, L., Serrano, O., and
567 Danobeitia, J.: Very high-resolution seismo-acoustic imaging of seagrass meadows (Mediterranean
568 Sea): Implications for carbon sink estimates, *Geophysical Research Letters*, 35, 2008.
- 569 de Macêdo Carneiro, P. B., de Lima, J. P., Bandeira, Ê. V. P., Neto, A. R. X., Barreira, C. de A. R., de
570 Souza Tâmega, F. T., Matthews-Cascon, H., Junior, W. F., and de Morais, J. O.: Structure, growth and
571 CaCO₃ production in a shallow rhodolith bed from a highly energetic siliciclastic-carbonate coast in
572 the equatorial SW Atlantic Ocean, *Marine environmental research*, 166, 105280, 2021.
- 573 Macreadie, P. I., Anton, A., Raven, J. A., Beaumont, N., Connolly, R. M., Friess, D. A., Kelleway, J. J.,
574 Kennedy, H., Kuwae, T., Lavery, P. S., and others: The future of Blue Carbon science, *Nature*
575 *communications*, 10, 3998, 2019.
- 576 Mao, J., Burdett, H. L., McGill, R. A., Newton, J., Gulliver, P., and Kamenos, N. A.: Carbon burial over
577 the last four millennia is regulated by both climatic and land use change, *Global Change Biology*, 26,
578 2496–2504, 2020.
- 579 Mao, J., Burdett, H., and Kamenos, N.: Efficient carbon recycling between calcification and
580 photosynthesis in red coralline algae, *Biology Letters*, 20, 2024.
- 581 Middelburg, J. J.: Reviews and syntheses: to the bottom of carbon processing at the seafloor,
582 *Biogeosciences*, 15, 413–427, 2018.
- 583 Moranta, J., Barberá, C., Druet, M., and Zaragoza, N.: Caracterización ecológica de la plataforma
584 continental (50-100 m) del canal de Menorca. Informe final área LIFE+ INDEMARES
585 (LIFE07/NAT/E/000732), Instituto Español de Oceanografía-Centro Oceanográfico de Baleares
586 (Palma), 2014.
- 587 Nellemann, C. and Corcoran, E.: Blue carbon: the role of healthy oceans in binding carbon: a rapid
588 response assessment, UNEP/Earthprint, 2009.
- 589 Neto, J. M., Bernardino, A. F., and Netto, S. A.: Rhodolith density influences sedimentary organic
590 matter quantity and biochemical composition, and nematode diversity, *Marine Environmental*
591 *Research*, 171, 105470, 2021.

- 592 Olmstead, S. A. and Andrus, C. F. T.: Growth characterization of mesophotic rhodoliths in the northern
593 Gulf of Mexico using radiocarbon dating, *Palaeogeography, Palaeoclimatology, Palaeoecology*, 654,
594 112438, 2024.
- 595 Rendina, F., Kaleb, S., Caragnano, A., Ferrigno, F., Appolloni, L., Donnarumma, L., Russo, G. F.,
596 Sandulli, R., Roviello, V., and Falace, A.: Distribution and characterization of deep rhodolith beds off
597 the Campania coast (SW Italy, Mediterranean Sea), *Plants*, 9, 985, 2020.
- 598 Rendina, F., Donnarumma, L., Ferrigno, F., and Russo, G. F.: Biodiversity of Mediterranean
599 mesophotic rhodolith beds: Macrofaunal community composition and structure (SW Italy), *Continental
600 Shelf Research*, 105682, 2026.
- 601 Riosmena-Rodríguez, R., Nelson, W., and Aguirre, J.: *Rhodolith/maërl beds: a global perspective*,
602 Springer, 2017.
- 603 Schubert, N., Tuya, F., Peña, V., Horta, P. A., Salazar, V. W., Neves, P., Ribeiro, C., Otero-Ferrer, F.,
604 Espino, F., Schoenrock, K., and others: “Pink power”—the importance of coralline algal beds in the
605 oceanic carbon cycle, *Nature Communications*, 15, 8282, 2024.
- 606 Tabone, L., Knittweis, L., Aguilar, R., Alvarez, H., Borg, J. A., Garcia, S., Schembri, P. J., and Evans,
607 J.: Habitat characterization, anthropogenic impacts and conservation of rhodolith beds off southeastern
608 Malta, *Aquatic Conservation: Marine and Freshwater Ecosystems*, 34, e4148, 2024.
- 609 Tauran, A., Dubreuil, J., Guyonnet, B., and Grall, J.: Impact of fishing gears and fishing intensities on
610 maerl beds: An experimental approach, *Journal of Experimental Marine Biology and Ecology*, 533,
611 151472, 2020.
- 612 Teichert, S.: Attached and free-living crustose coralline algae and their functional traits in the
613 geological record and today, *Facies*, 70, 8, 2024.
- 614 Trégarot, E., D’Olivo, J. P., Botelho, A. Z., Cabrito, A., Cardoso, G. O., Casal, G., Cornet, C. C., Cragg,
615 S. M., Degia, A. K., Fredriksen, S., and others: Effects of climate change on marine coastal
616 ecosystems—A review to guide research and management, *Biological Conservation*, 289, 110394, 2024.
- 617 Tuya, F., Schubert, N., Aguirre, J., Basso, D., Bastos, E. O., Berchez, F., Bernardino, A. F., Bosch, N.
618 E., Burdett, H. L., Espino, F., and others: Levelling-up rhodolith-bed science to address global-scale
619 conservation challenges, *Science of The Total Environment*, 164818, 2023..
- 620 Van Der Heijden, L. and Kamenos, N. A.: Reviews and syntheses: calculating the global contribution of
621 coralline algae to total carbon burial, *Biogeosciences*, 12, 6429–6441, 2015.
- 622 Wilson, S., Blake, C., Berges, J. A., and Maggs, C. A.: Environmental tolerances of free-living coralline
623 algae (maerl): implications for European marine conservation, *Biological conservation*, 120, 279–289,
624 2004.
- 625